PARAMETRIC PERFORMANCE OF CIRCUMFERENTIALLY GROOVED HEAT PIPES WITH HOMOGENEOUS AND GRADED-POROSITY SLAB WICKS AT CRYOGENIC TEMPERATURES

M. Groll*, R. B. Pittman**
Ames Research Center, NASA
Moffett Field, California, 94035, U.S.A.
and
J. E. Eninger
TRW Systems Group
Redondo Beach, California, 90278, U.S.A.

ABSTRACT

A recently developed, potentially high-performance nonarterial wick has been extensively tested. This slab wick has an axially varying porosity which can be tailored to match the local stress imposed on the wick. The purpose of the tests was to establish the usefulness of the graded-porosity slab wick at cryogenic temperatures between 110 K and 260 K, with methane and ethane as working fluids. For comparison, a homogeneous (i.e., uniform porosity) slab wick was also tested. The tests included:

- Maximum heat pipe performance as a function of fluid inventory.
- Maximum performance as a function of operating temperature.
- Maximum performance as a function of evaporator elevation.
- Influence of slab wick orientation on performance.

The experimental data were compared with theoretical predictions obtained with the computer program GRADE.

BACKGROUND AND OBJECTIVES

High transport capability in heat pipes operating near room temperature can be attained with the use of arteries, which simultaneously provide high capillary pressure and low flow resistance for the condensed liquid. Arterial heat pipes, however, have several disadvantages, especially if they are also gas-loaded variable-conductance heat pipes. In fact, arteries will not function at all for ammonia variable-conductance heat pipes, evidently because of pressure fluctuations that occur as a result of instability of the gas front /1/. With fluids that can be used (e.g., methanol), priming foils /2/ are required to vent the noncondensible gas and rigid leveling requirements are necessary during test to prime the arteries.

---

*National Research Council Associate
**Engineering Co-op Program, University of California, Davis

Conventional, nonarterial heat pipes are, in general, more reliable and easier to test than arterial heat pipes; however, they have a far lower heat transport capability. Therefore, a high-performance nonarterial wick was developed by optimally varying its porosity along its length. A conventional wick whose porosity is uniform along its length has an unnecessarily high capillary-pressure limit, and, hence, an unnecessarily low permeability everywhere except at the evaporator end, where the limit is reached at the maximum heat load. By varying the porosity, the capillary-pressure limit is only as high as required to sustain the local vapor-liquid pressure difference and, thus, the permeability is as high as possible everywhere along the length of the wick. The potential increase in performance of such a graded-porosity wick depends on the particular application, but it is typically greater than a factor of two /3/.

Despite the fact that the original goal was to develop a high-performance nonarterial, all-aluminum heat pipe for use with ammonia at near-room temperatures, the need for all-stainless-steel heat pipes for use with cryogenic working fluids, like ethane, methane, nitrogen, and oxygen was also recognized. The particular objective of this development was to demonstrate the performance of a graded-porosity wick heat pipe with cryogenic working fluids and to compare it (a) with the performance of an optimized homogeneous wick heat pipe, and (b) with theoretical predictions based on the computer program GRADE /4,5/.

DESCRIPTION OF INVESTIGATED CRYOGENIC HEAT PIPES

Two stainless-steel cryogenic heat pipes were developed: one with a graded-porosity wick ("G" wick), and the other with a homogeneous wick ("H" wick). The length of the heat pipes is 98 cm with 15-cm evaporator and condenser sections. The tubes are made of PH 15-7 Mo stainless steel. The outside diameter is 1.27 cm and the wall thickness is 0.7112 mm. The tubes are circumferentially threaded with 40 grooves/cm. The groove opening is 0.178 mm and the included angle is 38°.

Both the "G" and the "H" wick were designed for either methane at 150 K or ethane at 236 K. At these temperatures, methane and ethane have nearly identical heat pipe properties, as shown in Figs. 1, 2, and 3. Therefore, a single wick design can be used for both fluids. The predicted optimum porosity for the "H" wick (Fig. 4) is 86.3%. The optimum volume density (1-porosity) variation for the "G" wick is shown in Fig. 5. In Figs. 4 and 5 the geometrical dimensions of the wicks are also indicated. The wicks were designed and optimized to self-prime with the slab oriented horizontally at an evaporator elevation of 0.25 cm.

The calculated fluid inventories for the nominal operating temperatures (150 K for methane and 236 K for ethane) and for fill charges between 70% and 130% are given in Table 1. The temperature dependence of the fluid inventory for a given fill charge of 95% (see Optimum Fluid Inventory under EXPERIMENTS) is shown in Table 2. The fluid inventory is difficult to predict as the wick cross section is not accurately known. When the wick is inserted into the tube, it is deformed to an extent that cannot be determined.

Table 1: Fluid Inventory as a Function of Percent-Fill Charge, at Nominal Temperatures.

Fill charge	70	80	90	100	110	120	130	%
Methane "G"	11.12	12.70	14.29	15.88	17.47	19.06	20.64	g
at 150 K "H"	11.52	13.16	14.81	16.45	18.10	19.74	21.39	g
Ethane "G"	14.41	16.46	18.52	20.59	22.64	24.70	26.74	g
at 236 K "H"	14.93	17.06	19.20	21.33	23.46	25.60	27.73	g

Table 2: Fluid Inventory as a Function of Operating Temperature, at Nominal Fill Charge of 95%.

Temperature	110	120	130	140	150	160	170			K
Methane "G"	16.95	16.48	16.02	15.58	15.13	14.73	14.21			g
Temperature	170	180	190	200	210	220	236	240	260	K
Ethane "G"	22.50	22.01	21.55	21.11	20.66	20.23	19.60	19.46	18.83	g

As some experimental data obtained from ammonia "G" and "H" wick heat pipes are also presented, their brief description is given below. These heat pipes are 180 cm long, with 60-cm-long evaporator, adiabatic, and condenser sections. The 6061-T6 aluminum tubes have an outside diameter of 1.27 cm and a wall thickness of 0.889 mm. Their threads are identical to those of the cryogenic heat pipes. The optimum porosity of the homogeneous aluminum-fiber slab (0.521 cm thick, 0.127-mm fiber diameter) was calculated to be 85.5%. The optimum porosity of the "G" wick (0.457 cm thick) varied from 60.5% at the evaporator end to 84.5% at the condenser end. The wicks were designed and optimized to self-prime with the slab oriented horizontally at an evaporator elevation of 0.5 cm. The nominal temperature is 294 K and the calculated fluid inventory for 110% fill charge (10% to account for fillets) is 46.90 g for the "G" wick heat pipe and 56.40 g for the "H" wick heat pipe.

HEAT PIPE INSTRUMENTATION AND TEST SETUP

Heat Pipe Instrumentation

The heat pipe instrumentation is schematically shown in Fig. 6. A nichrome heater ribbon, insulated with Kapton foil, is wrapped around the evaporator. Two separate heaters are connected in series. Space is thereby provided for three thermocouples (TCs 4, 5, and 6) in the middle of the evaporator section. The heated evaporator length is approximately 14 cm. The copper-constantan thermocouples (TCs) are spot welded to the stainless-steel heat pipe tube.

The TC beads are protected by RTV. TC locations for both the "G" and "H" wick heat pipes are displayed in Fig. 6.

Test Setup

A schematic diagram of the test setup is depicted in Fig. 7. The tests were carried out in a vacuum chamber with room-temperature walls. The vacuum system provides a vacuum of less than 10^{-5} torr. The heat pipe is mounted on a test fixture, with a support bracket at the evaporator end. The condenser end with the fill valve is held by the liquid-nitrogen-cooled condenser block made from copper. Six cartridge heaters, connected in parallel, are inserted into the condenser block to provide heat for sink temperature control. The test frame can be elevated or lowered by means of a vacuum-tight rotatable feedthrough. The frame and the heat pipe are leveled by means of the feedthrough and the bubble level on the frame. The tilt of the heat pipe is measured with the ruler which is attached to the frame and the theodolite-mirror system which is firmly fixed to the floor outside of the chamber. The heat pipe is well insulated with 20 to 30 layers of aluminized Mylar foil.

Data Reduction

The data (temperatures, voltage, current) are obtained by means of a digital data acquisition system. For further data reduction, a paper tape is punched as the data are printed. This tape is fed into a small computer and the reduced data are again printed out and also plotted. The data reduction essentially consists of averaging the evaporator and condenser temperatures and calculating evaporator and condenser temperature drops. The temperature drops used for final data analysis are:

Evaporator: $$\Delta T_1 = \langle T_1, T_2, T_3 \rangle - T_{AD} \quad (1)$$

$$\Delta T_2 = \langle T_4, T_5, T_6 \rangle - T_{AD} \quad (2)$$

Condenser: $$\Delta T_3 = T_{AD} - \langle T_{11}, T_{12}, T_{13}, T_{14}, T_{15} \rangle \quad (3)$$

where the brackets indicate average and T_{AD} is the adiabatic temperature. The most reliable TC was used for defining the adiabatic temperature. This was TC8 or TC9 as shown below:

T_{AD}	Case
T_8	Methane, Ethane } hysteresis test, "G" wick
T_9	Methane, fill charge optimization, "G" wick
	Methane, Ethane } $\dot{Q}$-vs-temperature test, "G" wick
	Methane, hysteresis test, "H" wick

EXPERIMENTS

Some Data From Ammonia Heat Pipes

Measured zero-elevation performances at 294 K were 182 W (corresponding to a heat transport capability of 21,840 W cm) for the "G" wick heat pipe and 157 W (corresponding to 18,840 W cm) for the "H" wick heat pipe. The measured performance of the "G" wick heat pipe is in reasonable agreement with the theoretical predictions. However, an old version of GRADE /4/ was used for the wick optimization, and the "G" wick was calculated to be everywhere too dense. Another computer run with an updated version of GRADE /5/ showed that the zero-elevation performance can be as high as 282 W (corresponding to 33,840 W cm) for an optimized "G" wick. The measured performance of the "H" wick was better than predicted at evaporator elevations above 0 cm. The performance increase of the (nonoptimized) "G" wick over the optimum "H" wick was only somewhat more than 10%, for horizontal operation. However, the cross section of the "G" wick was 13% less than that of the "H" wick, and the "G" wick was not optimum. Based on the potential performance of the optimized "G" wick, an improvement of about 80% over the performance of the somewhat thicker "H" wick for horizontal operation can be expected.

Test Program for Cryogenic Heat Pipes

Optimum fluid inventory

The maximum throughput and evaporator and condenser temperature drops of the methane-filled "G" wick heat pipe are measured as functions of fluid inventory for horizontal slab orientation, 150 K adiabatic (vapor) temperature, and 0.25-cm evaporator elevation. Two critical performance levels are considered. The "burnout" power is reached when the maximum evaporator temperature drop, either ΔT_1 or ΔT_2, has risen to 20 K. This definition of burnout power is used for all subsequent tests. The "dryout" power is reached when, for increasing power, either the ΔT_1 or ΔT_2 curve shows a significant change in slope.

The leveled heat pipe is first cooled down to the desired operating temperature, and allowed to prime for 30 min. Then the heat pipe is elevated to 0.25-cm evaporator elevation. Power is added to the evaporator heaters in 4- to 5-W increments, which are reduced to 2- to 3-W increments when the expected burnout is approached. After burnout has been obtained, the heat pipe is allowed to warm up to room temperature, removed from the chamber, and vented to the next fill charge. From the results of these tests, an "optimum" or nominal fill charge can be defined on the basis of a tradeoff between performance and temperature drops.

Performance as function of operating temperature

The temperature dependence of performance is measured for the "G" wick heat pipe (filled with the nominal fluid inventory), for horizontal wick orientation and at an evaporator elevation of 0.25 cm. The leveled heat pipe is cooled down to the minimum operating temperature, and the test procedures described above are repeated. After the heat pipe is removed from the chamber, it is vented to contain the same nominal fill charge at the next higher operating temperature.

Performance as function of evaporator elevation (hysteresis tests)

These tests are carried out for the "G" wick heat pipe with methane (wick horizontal and vertical) and ethane (wick horizontal) as working fluids, with the nominal (95%) fluid inventory and at nominal operating temperatures (150 K for methane, 236 K for ethane). For comparison, these tests are also carried out with the "H" wick heat pipe, filled with methane (fill charge 105% for horizontal wick orientation and 100% for vertical wick orientation) at the nominal operating temperature of 150 K.

The test cooldown, priming, elevation, and power incrementing steps are as described above. However, 1- to 3-W increments, depending on evaporator elevation, are used when expected burnout is approached. After burnout has been obtained, the power is reduced in 2- to 3-W increments until the heat pipe recovers. Recovery occurs when the largest evaporator temperature difference is not more than the respective difference before burnout; that is, the evaporator temperatures have dropped to their preburnout value, indicating that the evaporator has been rewetted. The heat pipe is allowed to stablize at this condition for 5 to 20 min. Thereafter, power is increased in the same increments as described above until a burnout is obtained a second time. Before testing at the next evaporator elevation, the heat pipe is again leveled and allowed to prime for 30 min.

Theoretical predictions

All theoretical predictions are made by means of the computer program GRADE. As the present version of GRADE does not account for excess liquid, the fill charge optimization (variation) cannot be done on the computer. Moreover, all other calculations are carried out with a 100% fill charge.

Determination of evaporator and condenser film coefficients

Equation (4) is used to determine the evaporator and condenser film coefficients, h, from the experimental data.

$$h = \frac{\dot{Q}}{A} \cdot \frac{1}{\Delta T^1} \tag{4}$$

where $\dot{Q}$ is relatively low power, for which a linear relation ΔT^1 vs $\dot{Q}$ approximately holds; A is the internal heat transfer area, which depends on the internal tube diameter and the respective evaporation and condensation surfaces (which are blocked by the slab wick); and ΔT^1 is the temperature drop in evaporator or condenser, ΔT, minus the temperature drop across heat pipe wall, ΔT_w. In the evaporator, the largest of the following temperature drops is used:

$$\Delta T_1 = \langle T_1, T_2, T_3 \rangle - T_8 \tag{5}$$

$$\Delta T_2 = \langle T_4, T_5, T_6 \rangle - T_8 \tag{6}$$

In the condenser, the following expression is used:

$$\Delta T_3 = T_8 - \langle T_{12}, T_{13}, T_{15} \rangle \tag{7}$$

Results and Comparison With Theoretical Predictions

Optimum fluid inventory

The fill-charge optimization, as shown in Fig. 8, covers a range from 130 to 80%. Between 110 and 80%, the maximum power varies nearly linearly with fill charge, whereas over 110%, there is a greater-than-first-power dependence. This is attributed to the increasing effect of fillet flow which bypasses the wick. The dryout and burnout curves are nearly parallel and close to each other. This indicates that the transition from a moderately dried-out state to burnout (with either stable or unstable serious superheating of the evaporator) occurs in a small power range. The performance throughout is lower than expected, especially the 100% fill-charge data, Figs. 8 and 9. It is assumed that this is caused by the fact that, at higher powers, the circumferential grooves no longer can pump sufficient liquid away from the wick. This means that burnout is determined by a groove dry out rather than by a wick failure. By optimizing groove dimensions, this limitation can be prevented. Another reason for the low performance is that the wick did not fit tightly into the heat pipe tube, and might also have become deformed during insertion into the tube. Thereby, wick-groove contact is reduced, degrading the liquid supply to the evaporator surface. A nonuniform contact of the slab wick to the grooved wall is also indicated by the TC readings.

For high fill charges, apart from a local hot spot around TC2, the "G" wick, in most cases, dries out first in the middle of the evaporator (TCs 4, 5, 6). TC6 starts rising first, followed by TCs 5 and 4. With increasing power, TC4 soon becomes and remains highest, followed by TCs 6 and 5, which lie close together. It is possible to run the heat pipe in stable condition with this part of the evaporator seriously dried out ($\Delta T_2 \approx 80$ K). At higher powers, the far evaporator end starts to dry out. Similar to behavior at the mid-evaporator position, TC2 is always highest, then TC3 and 1, in this order, start to rise in temperature. A stable heat pipe operation can be maintained with the evaporator end seriously dried out ($\Delta T_1 \approx 30$ to 50 K). A further increase in power causes a fast runaway of the evaporator temperatures at a rate of 4 K/min to 10 K/min. The situation is somewhat different for small fluid inventories (80 to 100%). Here, TC2 no longer indicates a higher temperature, and the evaporator end starts to dry out very uniformly at relatively lower powers. Again, the middle of the evaporator dries out first, as described above.

For all fill charges, both the dryout and the burnout levels are determined by the temperature increase in the middle part of the evaporator.

Figure 8 further shows a distinct and similar fill-charge dependence of the evaporator and condenser temperature drops. The chief factor for the increase of ΔT with increasing fill charge can be attributed to the increasing maximum power. However, for underfill conditions, the evaporator temperature drops level off and tend to rise again at 80% fill charge. This can be explained by a superheating of the evaporator due to permanent deficiency of liquid. The condenser temperature drop falls off sharply for fill charges under 100%. It also seems to level off at 80% fill charge. However, the absolute value is so small (0.5 K) that the temperature precision of the measurements is exceeded.

The conclusion is that a fill charge of 100% or somewhat less can be considered to be optimum. In this range, the overall temperature drops are reasonably small and the reduction in maximum performance is tolerable. Therefore, 95% fill charge was chosen as the nominal value for all tests with the "G" wick heat pipe.

Performance as function of operating temperature

The measured data can be represented by curves (Fig. 9 for methane and Fig. 10 for ethane), the shape of which is in excellent agreement with the shape of the theoretically predicted curves, though they are considerably lower throughout the entire temperature range. There is also good agreement with the figures of merit (Fig. 1) of methane and ethane. These facts indicate that, for both working fluids and the temperature range covered, the liquid pressure drop strongly dominates, and vapor flow pressure drops can be neglected.

Performance as function of evaporator elevation (hysteresis tests)

The results for the "G" wick heat pipe with methane and ethane as working fluids (nominal fill charge of 95%) are depicted in Figs. 11, 12, and 13. The results for the "H" wick heat pipe with methane as working fluid (fill charge 105% for horizontal wick orientation, and 100% for vertical wick orientation) are shown in Figs. 14 and 15. In Fig. 14, the performance prediction for the optimized "H" wick is also included. The performance predictions for the actual porosity distribution of the "G" wick (wick horizontal) are included in Figs. 11 and 13. That the slope of the predicted power-vs-elevation curve is not constant is due to the fact that, for a "G" wick, capillary failure does not always initiate at the evaporator end.

The performance of the "G" wick heat pipe is significantly higher when the slab wick is oriented vertically, compared to the horizontal wick orientation; but, in both cases, the extrapolated experimental curves are far below the predicted curve. The reasons for the low measured performance have been discussed earlier. The superior performance of the vertical wick seems to be due to the fact that liquid supply to the circumferential grooves is somewhat easier to achieve when the wick is vertical. The measured data indicate that the wick has an excellent repriming capability, at least up to an elevation of 2 to 3 cm, and probably until close to the zero-load elevation. However, some data points reveal a considerably lower second burnout. This is attributed to the fact that, in these cases, the heat pipe was not fully recovered before beginning the second burnout run. For most of these cases, power had not been reduced sufficiently and/or the time period at recovery power had not been long enough to reduce the evaporator temperature sufficiently. The relevant evaporator temperature differences ΔT_1 and ΔT_2 are indicated in Figs. 11, 12, and 13.

The data for the horizontal wick orientation indicate a fillet or puddle flow effect at low elevations. At first glance, this seems to be rather improbable, since the fill charge is only 95%. However, in fibrous wicks, as stress builds up, partial desaturation sets in as the larger pores give up fluid. This is especially pronounced when approaching high loads. Secondary reasons for this effect might be an imperfect wick-groove contact and the fact that, when calculating the fluid inventory, the circumferential grooves were assumed to be completely filled with liquid. For the vertical wick orientation, the fillet flow effect is less pronounced.

The "H" wick heat pipe has a performance superior to that of the "G" wick heat pipe. The overriding reason for this unexpected fact is that the "G" wick is designed to operate at high stress (in the evaporator section) beyond the pumping capability of the grooves, whereas the much less dense "H" wick operates at a lower stress which the grooves can handle. Other reasons might be that the groove contact of the "G" wick is not perfect and that the "H" wick has a larger cross section.

The experimental data for the horizontal wick are in good agreement with theory for higher elevations. The increasingly greater deviations at small elevations can be attributed to the slight overcharge of 105%. If a linear extrapolation to zero-elevation is made, based on the high-elevation data points, agreement between experiments and theory becomes much better. Comparison of the vertical wick measurements with theory shows good agreement, also at zero-elevation. This is believed to be due to the 100% fill charge, which apparently does not lead to any fillet flow in this case. For the horizontal wick orientation, nearly perfect repriming could be achieved for all elevations. The results are somewhat worse for the vertical wick. However, this can be explained by a starting of the second burnout run from a not fully recovered state.

Determination of evaporator and condenser film coefficients

Evaporator and condenser film coefficients were derived from measured data, as described in the test program section. Despite a considerable scatter in data, curves can be extrapolated which give a rough indication of the magnitude of the film coefficients (Figs. 16 and 17). The condenser film coefficient of the "G" wick heat pipe reveals a distinct dependence on fill charge. It increases by a factor of six when the fill charge decreases from 130 to 80%. The evaporator film coefficient, which is much smaller, is essentially independent of fill charge. For the "H" wick, the fill-charge dependence was not investigated. As depicted in Fig. 16, for about 100% fill charge, the evaporator film coefficient of the "H" wick heat pipe is somewhat higher than the condenser film coefficient, and it is considerably higher than the evaporator film coefficient of the "G" wick. The condenser film coefficient, however, is remarkably smaller than that of the "G" wick heat pipe.

The temperature dependence and the relative values of the film coefficients for methane and ethane (Fig. 17) cannot be convincingly explained. The film coefficients for methane and ethane differ considerably, which is not in accordance with the thermal conductivities of the liquids (Fig. 3). Secondly, the evaporator coefficient for methane is much smaller than the condenser coefficient (0.085 W cm^{-2} K^{-1} and 0.44 W cm^{-2} K^{-1}, respectively, at a nominal temperature of 150 K). For ethane, the results are exactly opposite. There, at a nominal temperature of 236 K, the evaporator and condenser coefficients are 0.18 W cm^{-2} K^{-1} and 0.13 W cm^{-2} K^{-1}, respectively. The coefficients for ethane show a temperature dependence which can be attributed to the temperature dependence of the liquid conductivity. For methane, however, the evaporator film coefficient is essentially temperature-independent, whereas the temperature dependence of the condenser film coefficient is very strong. It increases by a factor of 4.8 between 170 K and 110 K, whereas the liquid conductivity increases by a factor of only 1.9.

CONCLUSIONS

The test program was only partially successful. The optimum performance of a graded-porosity wick heat pipe was not satisfactorily demonstrated at cryogenic temperatures. The test results were below the theoretical predictions, by a factor of 1.3 (ethane) to 1.8 (methane), for nominal test conditions of 0.25-cm evaporator elevation and 236 K (ethane) and 150 K (methane) operating temperatures. The optimized homogeneous wick heat pipe, however, performed very well. Its performance was in good agreement with theoretical predictions, and was considerably higher than that of the graded-porosity wick heat pipe.

There is strong evidence that the grooves of the investigated cryogenic graded-porosity wick heat pipe were not optimally matched to the slab wick. This is a crucial point, and more attention must be given to the matching of the capillary capabilities of the grooves and the wick.

Theoretical predictions and experimental results indicate that both the optimized homogeneous and the graded-porosity wick heat pipes have the potential for high throughput and excellent tilt performance, when using methane and ethane as cryogenic working fluids. Concerning the tilt capability, both heat pipes are far superior to conventional axial groove heat pipes. With respect to performance, the optimized homogeneous wick is comparable with conventional axial groove heat pipes. The optimized graded-porosity wick heat pipe, though not yet fully demonstrated, promises a potentially high performance which is superior to that of conventional axial groove heat pipes and may be strongly competitive with that of improved axial groove designs. This high-performance potential, however, can only be realized when the grooves are matched to the slab wick. This potential is demonstrated by the excellent performance of the ammonia graded-porosity wick heat pipe. The graded-porosity wick also offers favorable application in gas-controlled thermal control heat pipes.

REFERENCES

/1/ W. T. Anderson, D. K. Edwards, J. E. Eninger, B. D. Marcus: Variable Conductance Heat Pipe Technology - Final Research Report. NASA CR-114750, March 1974.

/2/ J. E. Eninger: Meniscus Coalescence as a Mechanism for Venting Noncondensible Gas From Heat Pipe Arteries. AIAA Paper No. 74-748, AIAA/ASME Thermophysics and Heat Transfer Conference, Boston, Massachusetts, July 1974.

/3/ J. E. Eninger: Capillary Flow Through Fibrous Heat Pipe Wicks. AIAA Paper No. 75-661, AIAA 10th Thermophysics Conference, Denver, Colorado, May 1975.

/4/ J. E. Eninger: Computer Program GRADE for Design and Analysis of Graded-Porosity Heat Pipe Wicks. NASA CR-137618, August 1974.

/5/ J. E. Eninger: Extensions to GRADE. Contract No. NAS 2-8310, August 1975.

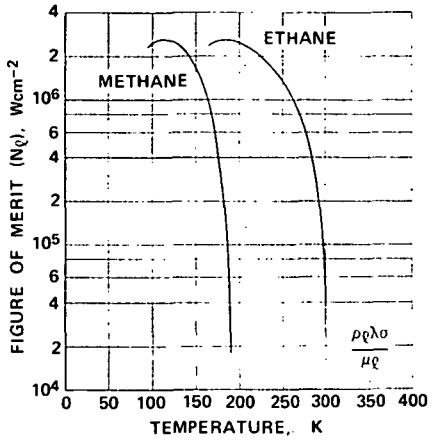

Fig. 1 Figure of merit of methane and ethane.

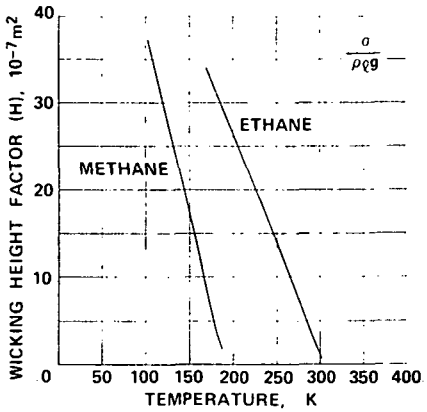

Fig. 2 Wicking height factor of methane and ethane.

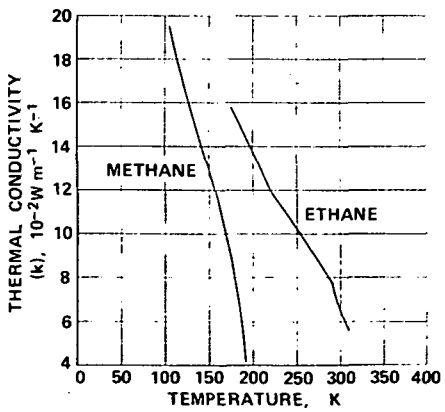

Fig. 3 Thermal conductivity of methane and ethane.

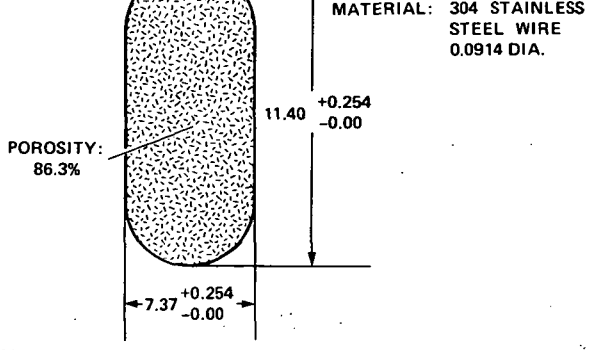

Fig. 4 Cross section of homogeneous wick.

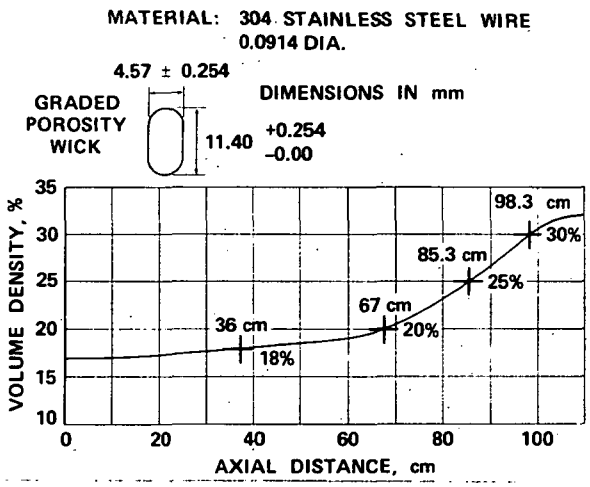

Fig. 5 Axial density distribution and cross section of graded-porosity wick.

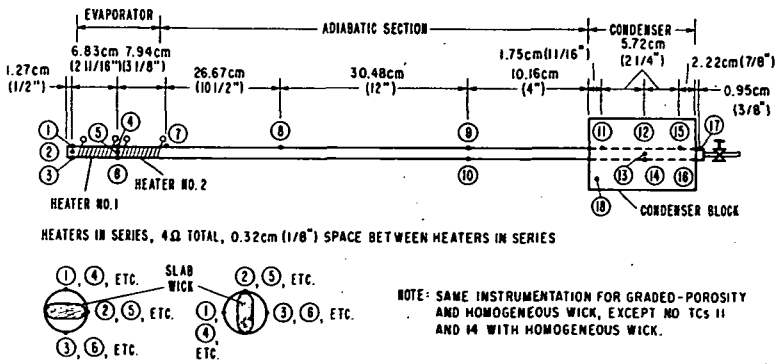

Fig. 6 Schematic drawing of heat pipe with instrumentation.

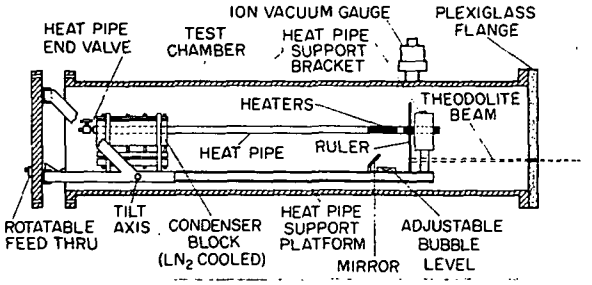

Fig. 7 Schematic drawing of cryogenic test setup.

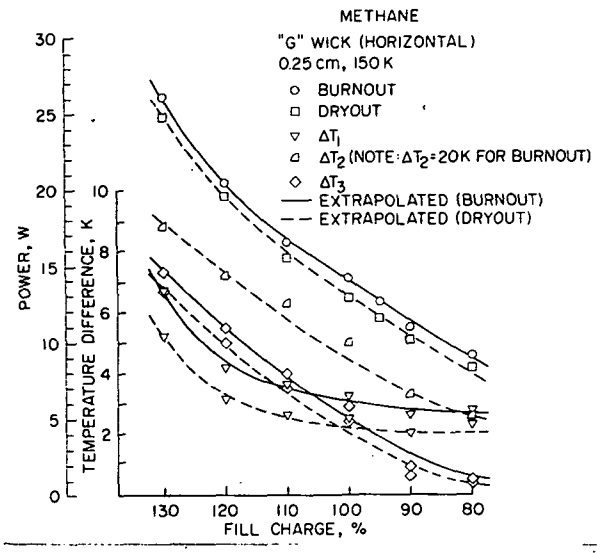

Fig. 8 Power vs. fill charge for methane "G" wick heat pipe.

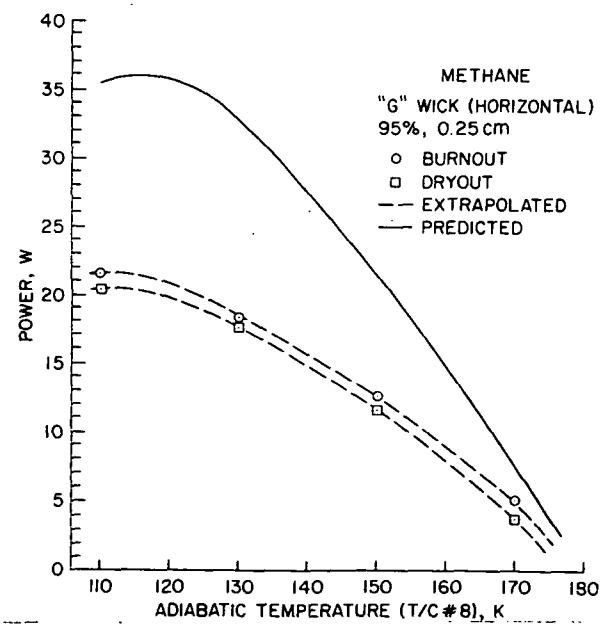

Fig. 9 Power vs. temperature for methane "G" wick heat pipe.

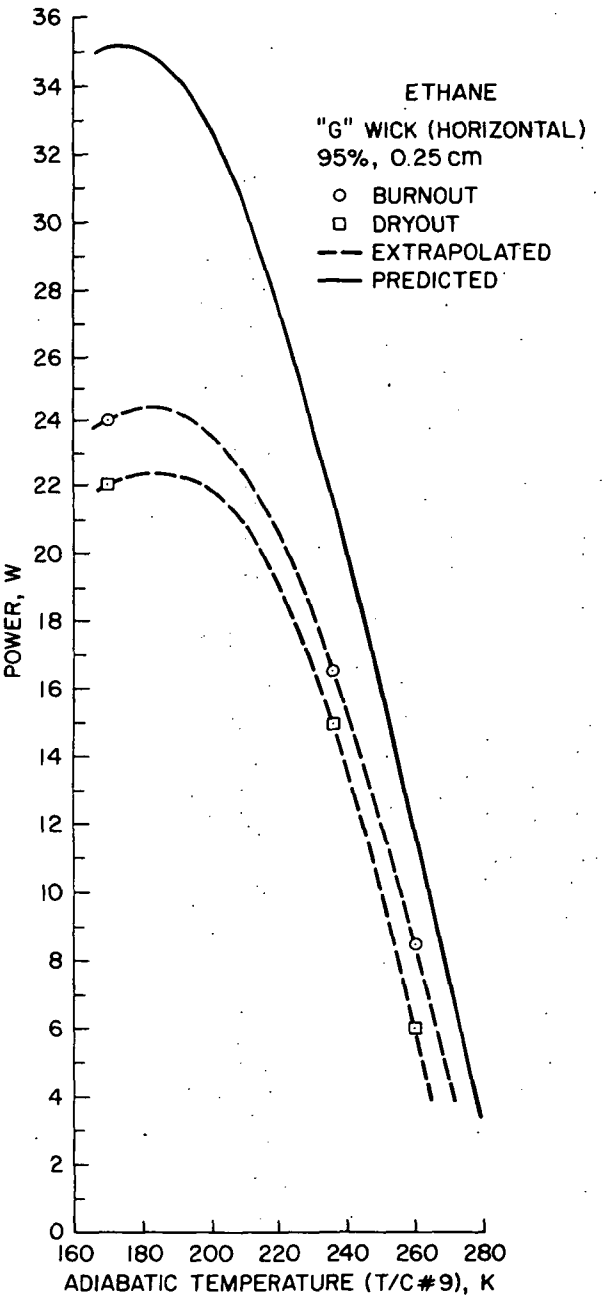

Fig. 10 Power vs. temperature for ethane "G" wick heat pipe.

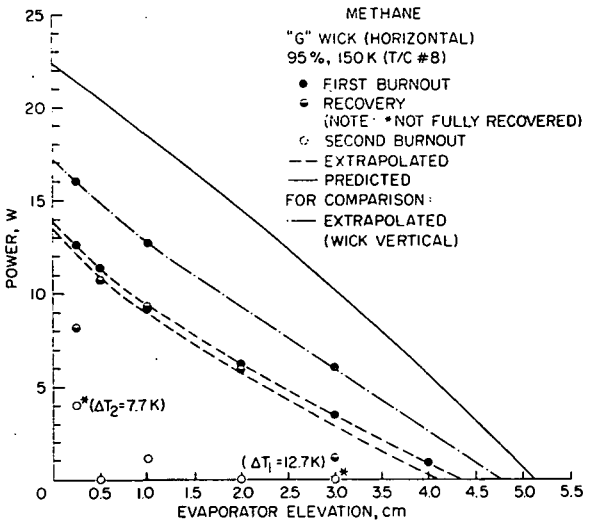

Fig. 11 Power vs evaporator elevation for methane "G" wick heat pipe (wick horizontal).

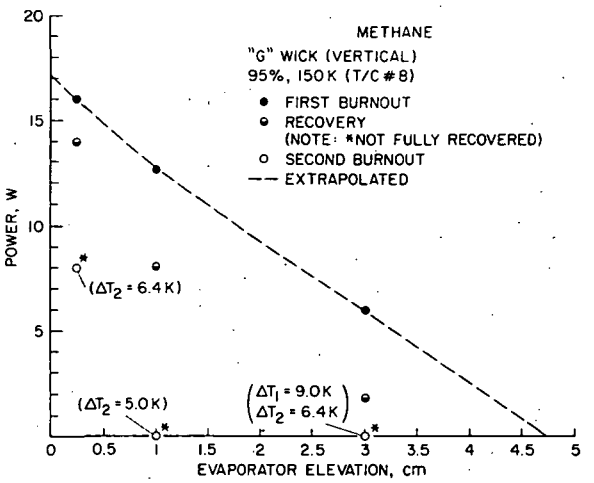

Fig. 12 Power vs evaporator elevation for methane "G" wick heat pipe (wick vertical).

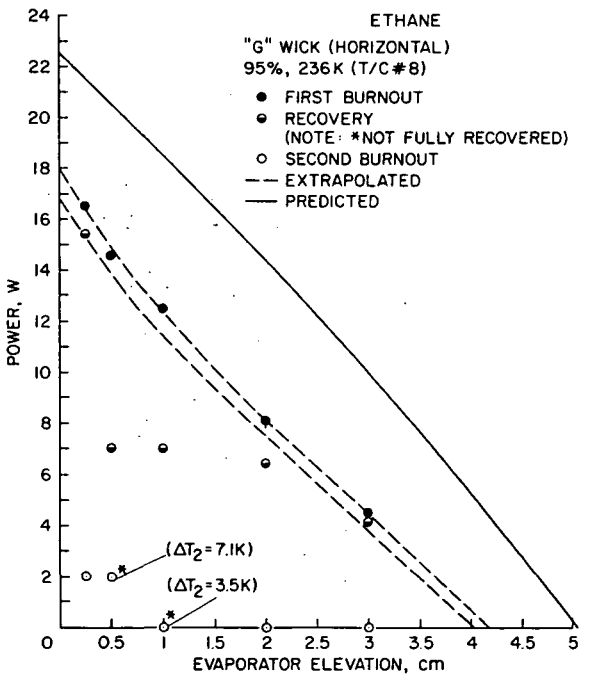

Fig. 13 Power vs evaporator elevation for ethane "G" wick heat pipe (wick horizontal).

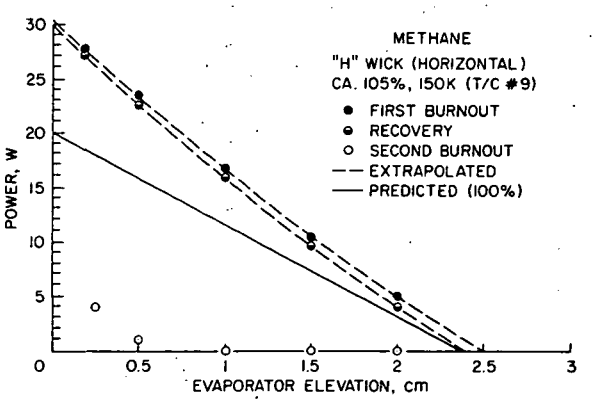

Fig. 14 Power vs evaporator elevation for methane "H" wick heat pipe (wick horizontal).

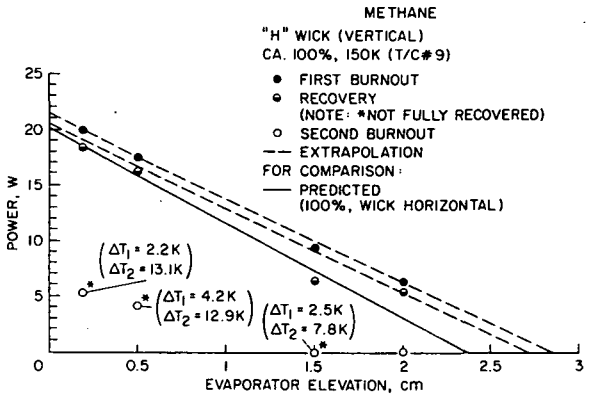

Fig. 15 Power vs evaporator elevation for methane "H" wick heat pipe (wick vertical).

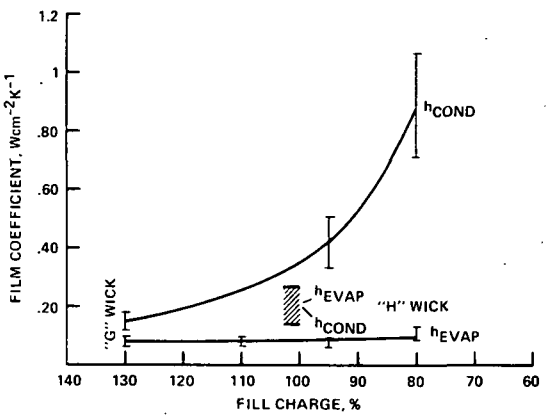

Fig. 16 Evaporator and condenser film coefficients vs fill charge for methane and ethane "G" wick heat pipes.

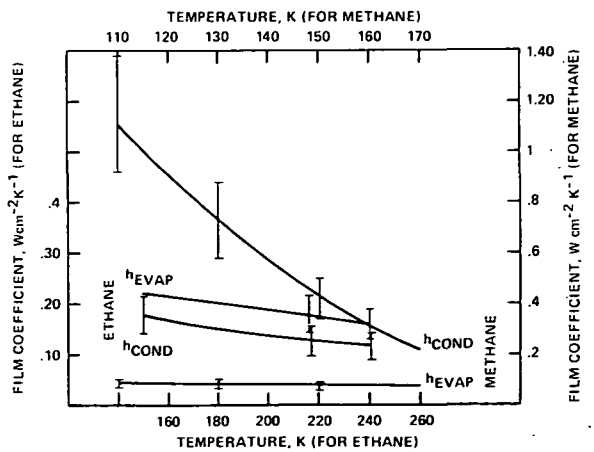

Fig. 17 Evaporator and condenser film coefficients vs temperature for methane and ethane "G" wick heat pipes.